BBA - Bioenergetics 1860 (2019) 699–707

Contents lists available at ScienceDirect

BBA - Bioenergetics

journal homepage: www.elsevier.com/locate/bbabio

Calculated vibrational properties of semiquinones in the A_1 binding site in photosystem I

Leyla Rohani[a], Hiroki Makita[a], Andrew Levitz[b], Maged Henary[b], Gary Hastings[a,*]

[a] Department of Physics and Astronomy, Georgia State University, Atlanta, GA, United States of America
[b] Department of Chemistry, Georgia State University, Atlanta, GA, United States of America

ARTICLE INFO

Keywords:
Photosynthesis
Photosystem I
Electron transfer
A_1
Time-resolved FTIR
ONIOM
Density functional theory

ABSTRACT

Time-resolved ($P700^+A_1^-$ – $P700A_1$) FTIR difference spectra have been obtained using photosystem I (PSI) particles with several different quinones incorporated into the A_1 protein binding site. Difference spectra were obtained for PSI with unlabeled and ^{18}O labeled phylloquinone (2-methyl-3-phytyl-1,4-naphthoquinone) and 2-methyl-1,4-naphthaquinone (2MNQ) incorporated, and for PSI with unlabeled 2,3-dimethyl-1,4-naphthoquinone (DMNQ) incorporated. (^{18}O – ^{16}O), (2MNQ – PhQ) and (DMNQ – PhQ) FTIR double difference spectra were constructed from the difference spectra. These double difference spectra allow one to more easily distinguish protein and pigment bands in convoluted difference spectra. To further aid in the interpretation of the difference spectra, particularly the spectra associated with the semiquinones, we have used two-layer ONIOM methods to calculate corresponding difference and double difference spectra. In all cases, the experimental and calculated double difference spectra are in excellent agreement. In previous two and three-layer ONIOM calculations it was not possible to adequately simulate multiple difference and double difference spectra. So, the computational approach outlined here is an improvement over previous calculations. It is shown that the calculated spectra can vary depending on the details of the molecular model that is used. Specifically, a molecular model that includes several water molecules that are near the incorporated semiquinones is required.

1. Introduction

In photosynthetic oxygen evolving organisms, solar energy is captured and converted in two separate membrane-spanning protein complexes called photosystem I and II (PSI and PSII). In both photosystems, light initiates the transfer of electrons, via a series of protein bound pigments, across the thylakoid membrane [1]. In PSI electron transfer (ET) can occur down either of two nearly symmetric branches, called the A- and B-branches [2]. The geometry of the ET cofactors in PSI is outlined in Fig. 1A.

Following light excitation of PSI, the $P700^+A_1^-$ secondary radical pair state is formed within ~50 ps [3,4]. ET from PhQ^- to F_X in PSI at room temperature (RT) is biphasic and is characterized by time constants of ~25 and 300 ns which are due to ET down the B- and A-branches, respectively [3–5]. The factors responsible for such a difference in time constants is not entirely clear [6].

At low temperature (LT, 77 K) ET in PSI occurs predominantly down the A-branch [7], and the main observable process in repetitive laser flash experiments is the recombination of the $P700^+A_{1A}^-$ radical pair state, with a lifetime of ~340 μs [5]. Experimentally, we have taken advantage of the simplified bioenergetics at 77 K to obtain highly sensitive time-resolved (TR) ($P700^+A_{1A}^-$ – $P700A_{1A}$) FTIR difference spectra (DS).

In PSI a phylloquinone molecule (PhQ) occupies the A_1 binding site [4,8], and acts as an intermediary in transferring electrons from A_0 to F_X (Fig. 1A). PhQ is a 2-methyl-3-phytyl-1,4-naphthoquinone. The PhQ that occupies the A_1 binding site in PSI has an extreme redox potential (E_m ~ −700 mV) [9]. It is in fact one of the most reducing quinones in all of biology [5,9,10]. The structural details of the A_1 binding site, and relevant pigment-protein interactions that bestow such a unique

Abbreviations: 2MNQ, 2-methyl-1,4-naphthaquinone; DFT, density functional theory; DAS, decay associated spectra; DS, difference spectra/spectrum/spectroscopy; DDS, double difference spectrum; DMNQ, 2,3-dimethyl-1,4-naphthaquinone; EE, electronic embedding; ET, electron transfer; FTIR, Fourier transform infrared; IR, infrared; LT, low temperature (~77 K); MM, molecular mechanics; ONIOM, our own N-layered integrated molecular orbital and molecular mechanics method; ME, mechanical embedding; PhQ, phylloquinone; PSI, photosystem I; PBRCs, purple bacterial reaction centers; QM, quantum mechanical; RT, room temperature (~298 K); *S6803*, *Synechocystis* sp. PCC 6803; TR, time resolved

* Corresponding author.
E-mail address: ghastings@gsu.edu (G. Hastings).

https://doi.org/10.1016/j.bbabio.2019.07.003
Received 17 February 2019; Received in revised form 3 June 2019; Accepted 10 July 2019
Available online 12 July 2019
0005-2728/ © 2019 Elsevier B.V. All rights reserved.

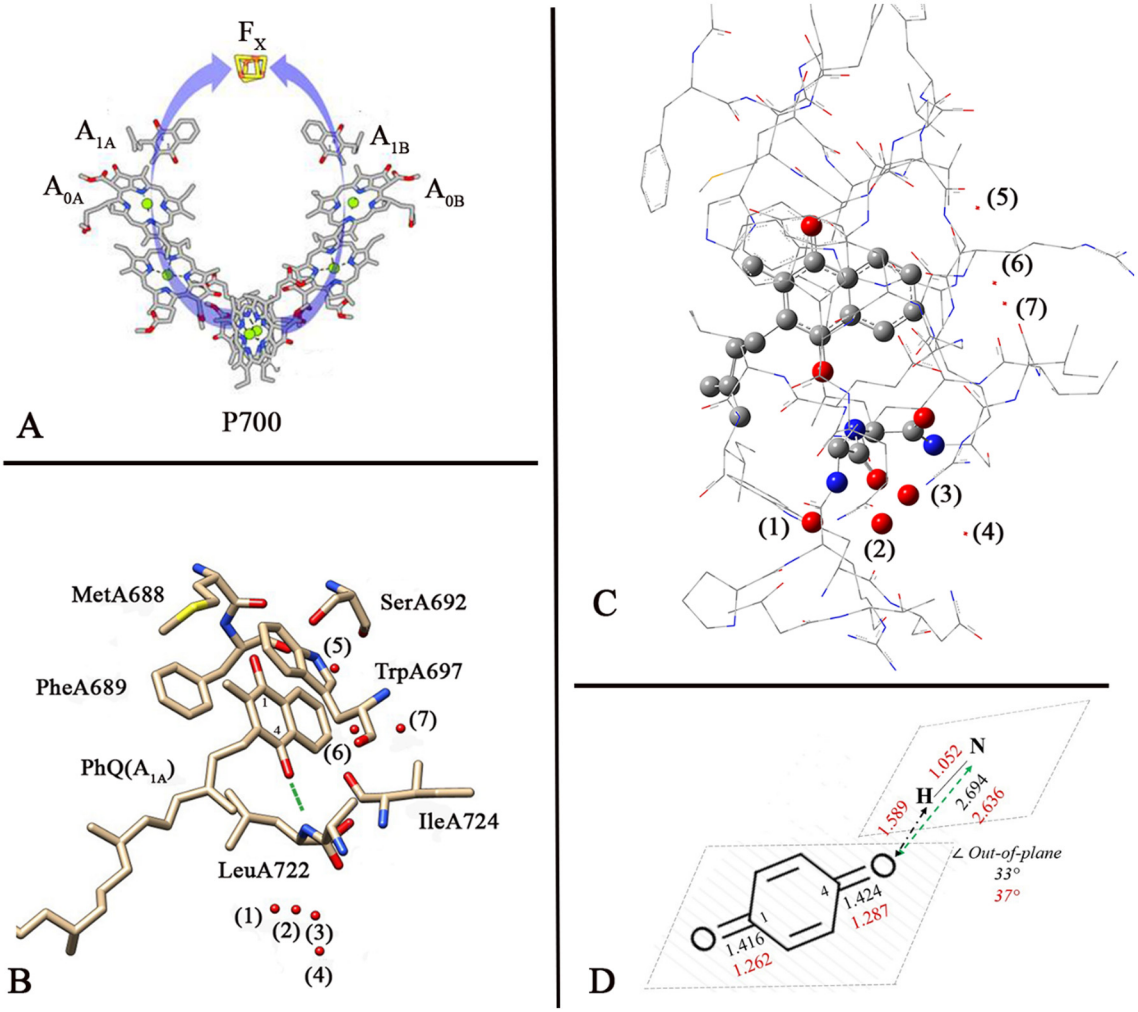

Fig. 1. (A) Arrangement of the ET cofactors in PSI. (B) View of PhQ in the A_{1A} binding site. H-bonding between the NH backbone of LeuA722 and the C_4═O oxygen atom of PhQ is shown (*green*). The oxygen atoms of seven nearby water molecules are also shown. Figure was generated using the 2.5 Å X-ray crystal structure of PSI from *Thermosynechococcus elongatus* (PDB 1JB0) [12]. (C) Two-layer molecular model used in ONIOM calculations. QM layer shown as ball and bond. MM layer as sticks. Hydrogen atoms are not shown. The oxygen atoms of the seven water molecules shown in (B) and (C) are: (1) A5018, (2) A5055, (3) A5031, (4) A5030, (5) A5043, (6) A5015, and (7) A5007. Water molecules (1), (2) and (3) were included in the QM layer. Carbon/nitrogen/oxygen atoms are grey/blue/red, respectively. (D) ONIOM calculated bond distances and angles. Black/Red: X-ray/Reduced (D) ONIOM calculated bond distances and angles. Black/Red: X-ray/Reduced PhQ. Only the quinonic part of the NQ ring is shown.

property to the bound PhQ are poorly understood [9]. The structure of PhQ in the A_{1A} binding site, along with nearby amino acids is outlined in Fig. 1B. The structure of PhQ on the B-branch is similar [11].

Fig. 1B shows the structure of PhQ and the surrounding amino acids in the A_1 binding site. The C_1═O group of PhQ is free from H-bonding, while the C_4═O group is H-bonded to the backbone NH group of LeuA722. The oxygen atoms of seven nearby water molecules (numbered 1–7) are also shown. Three of these water molecules (numbered 1–3) could be part of an H-bond network involving the backbone oxygen/nitrogen of SerA723/AlaA721, respectively. These water molecules are conserved in all available PSI crystal structures [12–14] and therefore likely serve an important structural function, and should therefore be included in most types of quantum chemical calculations of the properties of quinones in the A_1 binding site. In this manuscript we show that these water molecules are crucial components that need to be included in molecular models that are constructed in order to produce calculated spectra that agree well with all of the different experimental spectra.

FTIR DS has been widely used to study pigments in a wide range of protein binding sites [15–25]. This widespread use stems from the fact that the technique is sufficiently sensitivity to identify specific pigment-protein interactions and small changes in these interactions that occur upon reaction.

FTIR DS can be applied to the study of pigment-protein complexes in a time-resolved (TR) manner [26–31], and such an approach has been shown to be sensitive to the temporal changes in single molecular bonds of pigments in proteins [21,32–35].

TR FTIR DS at 77 K has been shown to be a useful technique for studying PSI with different quinones incorporated into the A_1 binding site [33]. The spectra obtained are complex, however, with many overlapping bands from multiple molecular components. To aid in the assignment of the experimentally observed bands, a computational method that can simulate pigment-protein interactions is required. Previously, density functional theory (DFT) based vibrational frequency calculations of asymmetrically H-bonded quinones in the gas phase has been a valuable aid in interpreting experimental FTIR DS [36]. However, it has been shown that those models do not adequately account for the protein environment surrounding the quinone [37,38].

Despite software developments, and the availability of high-performance computers, it is still difficult and time-consuming to calculate the spectroscopic properties of large molecular systems using purely quantum mechanical (QM) methods [39]. Dividing a large molecular

structure into multiple fragments, and using different levels of theory for the calculation of the different fragments is becoming common, with hybrid methods embedded in many types of commercially available software [39]. Such parsing techniques allow the most important parts of a molecular model to be treated using expensive QM methods, while the majority of the molecular model can be treated using inexpensive molecular mechanics (MM) methods. In this manuscript we utilize a two-layer ONIOM-type QM:MM method. ONIOM is an acronym for **O**ur own **N**-layered **I**ntegrated molecular **O**rbital and molecular **M**echanics method. Previously we have used a three-layer ONIOM-type QM:QM:MM method to calculate the vibrational properties of PhQ and 2MNQ in the A_1 binding site [40]. A relatively small molecular model was used in these calculations, and it was shown that in many instances the calculated spectra poorly modeled the experimental spectra [40].

In this manuscript TR ($P700^+A_{1A}^-$ – $P700A_{1A}$) FTIR DS at 77 K are obtained for PSI with PhQ, 2MNQ and DMNQ incorporated, and for PSI with ^{18}O labeled PhQ and 2MNQ incorporated. The band structure in the many different spectra contains a wealth of information on the structural properties of the bound quinones. This structural information can be accessed through interpretation and assignment of the bands in the spectra. To aid in spectral band interpretation and assignment we have used a two-layer ONIOM-type QM:MM method to calculate the vibrational properties of the different incorporated quinones. The molecular model used is considerably expanded compared to that used in previous calculations, especially in terms of the atomic composition of the QM layer. Using this more extensive molecular model we show a remarkable agreement between all calculated and experimental spectra.

2. Materials and methods

2.1. Sample preparation

PhQ and 2MNQ and all other chemicals were purchased from Sigma-Aldrich and used as received. Quinones were incorporated into the A_1 binding site using *menB*$^-$ PSI particles from *S6803*, as described previously [41]. In this manuscript we will refer to the binding site as A_1, and the quinone in the binding site will be referred to by name. 2-methyl,3-phytyl-1,4-naphthaquinone (PhQ) and 2-methyl-1,4-naphthaquinone (2MNQ) with both carbonyl oxygen atoms ^{18}O labeled were prepared and isotope incorporation levels were assessed as described previously [41]. 2,3-Dimethylnaphthoquinone (DMNQ) was synthesized from 2,3-dimethylnaphthalene as described previously [42].

2.2. FTIR spectral acquisition

Microsecond time-resolved step-scan (TRSS) FTIR DS, at 4 cm^{-1} spectral resolution, for the different PSI particles at 77 K were collected using a Bruker Vertex 80 FTIR spectrometer, as described previously [43]. Global analysis of the TRSS FTIR DS was undertaken using Glotaran [44]. The TRSS FTIR DS were fitted globally to multi-exponential functions, and decay-associated spectra (DAS) were constructed. At 77 K, the $P700^+A_1^-$ charge recombination has a lifetime of ~240–340 μs, and the DAS with such a lifetime we call [$P700^+A_1^-$ – $P700A_1$] FTIR DAS, and it is these DAS that are presented in this manuscript. As indicated previously [40], this global analysis procedure allows an easy separation of the signals of interest from heating induced artefactual signals that decay in ~15 μs (see Fig. S4 in reference [40]).

2.3. Molecular model construction

Molecular models were constructed using the PSI crystal structure from *Thermosynechococcus elongatus* (PDB file 1JB0) [12]. PhQ in the A_{1A} binding site was chosen. The molecular model consists of atoms that are within 12 Å of either carbonyl (C=O) oxygen atom of PhQ. This is a much larger molecular model than that considered previously [40]. The phytyl tail of PhQ was truncated to a 5-carbon unit [$CH_2CHC(CH_3)_2$. Hydrogen (H) atoms were added to the molecular model using GaussView 6 software [45]. Standard protonation states were used for all amino acids (amino acids included in the molecular model, and their charge state, are listed in Table S1).

Water molecules, and heavy atoms of the quinones, as well as all hydrogen atoms, were unconstrained. All other heavy atoms were constrained. The molecular model considered here is outlined in Fig. 1C. For modeling 2MNQ/DMNQ in the A_1 binding site, the truncated tail of PhQ is replaced by a hydrogen atom/methyl group, respectively. We have undertaken calculations for 2MNQ in the binding site with its methyl group both ortho and meta to the H-bonded C_4=O group. The backbone of AlaA721, LeuA722 and SerA723 (only the nitrogen atom) were included in the QM layer (Fig. 1C). Water molecules numbered 1–3 in Fig. 1B/C are involved in a complicated H-bond network, and are also included in the QM layer.

2.4. Calculations

ONIOM calculations were undertaken using Gaussian 16 software [46]. QM level calculations were undertaken using hybrid DFT methods, employing the B3LYP functional and the 6-31 + G(d) basis set. This combination has been shown to be appropriate for optimization and vibrational frequency calculations of semiquinones [47,48]. The MM layer was treated using UFF [49]. The QM and MM layers were connected using the link atom approach [39]. Geometry optimization of the two-layer model was undertaken using ONIOM methods employing electronic embedding (EE), which allows the electrostatic potential of the surrounding atoms to be included in the QM wave function [38].

The molecular model that was geometry optimized using ONIOM methods was then used in vibrational frequency calculations undertaken using the ONIOM method employing mechanical embedding. In this case no constraints were placed on the heavy atoms.

GaussView 6 software allows animations of the normal modes to be visualized. Mode assignments are based on inspection of these animations.

In the work reported here all normal mode frequencies and intensities are calculated. With both the frequency and intensity information IR stick spectra can be constructed. By convolving these stick spectra with a Gaussian function of 4 cm^{-1} half-width more realistic-looking spectra are constructed. We refer to these convolved stick spectra simply as absorption spectra.

In semiquinone calculations, a frequency scaling factor of 0.964 was used. This number is chosen to align calculated frequencies with the experimental bands observed at 1495 and 1415 cm^{-1} [33,40].

3. Results

TR ($P700^+A_1^-$ – $P700A_1$) FTIR DAS at 77 K were obtained for PSI particles with unlabeled and ^{18}O labeled PhQ incorporated, and for PSI with 2MNQ and DMNQ incorporated. By subtracting a photo-accumulated ($P700^+$ – P700) FTIR DS from the TR ($P700^+A_1^-$ – $P700A_1$) FTIR DAS, an (A_1^- – A_1) FTIR DS can be constructed [50]. Fig. 2 shows experimental (A_1^- - A_1) FTIR DS in the semiquinone spectral region (~1550–1390 cm^{-1}) for four quinones incorporated (*dotted lines*). Corresponding ONIOM calculated spectra are also shown (*solid lines*).

Fig. 3 shows (^{18}O – ^{16}O), ($2MNQ^-$ – PhQ^-), and ($DMNQ^-$ – PhQ^-) double difference spectra (DDS) that were constructed by subtracting TR ($P700^+A_1^-$ – $P700A_1$) FTIR DAS for PSI with PhQ incorporated from the ($P700^+A_1^-$ – $P700A_1$) FTIR DAS for PSI with the non-native quinone incorporated. Near identical DDS are obtained by using the (A_1^- – A_1) FTIR DS in Fig. 2 (*not shown*). Corresponding ONIOM calculated DDS are also shown in Fig. 3. The calculated and experimental DS in Fig. 2 and DDS in Fig. 3 are in excellent agreement.

Figs. 2 and 3 focus on spectra of the semiquinones, in the ~1520–1390 cm^{-1} region. Calculated and experimental DDS covering both the neutral and anion region (~1800–1390 cm^{-1}) are presented in

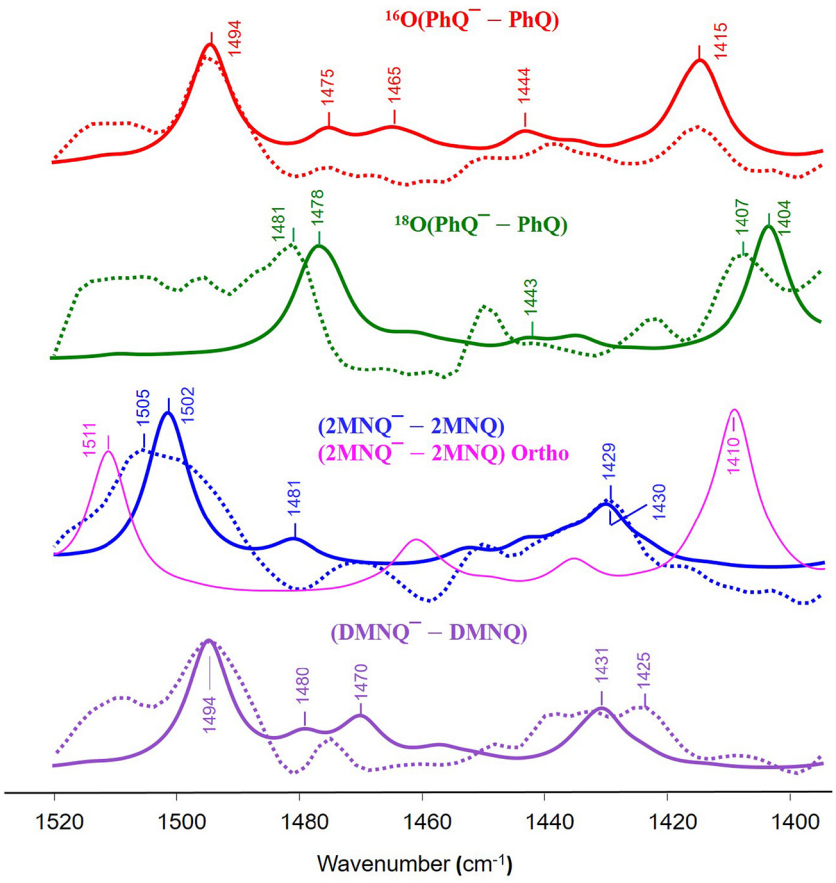

Fig. 2. ONIOM calculated DS in the 1550–1390 cm^{-1} region for molecular models with unlabeled (*red*) and ^{18}O labeled (*green*) PhQ^- in the A_1 binding site. Calculated spectra are also shown for PSI with $2MNQ^-$ (*blue*) and $DMNQ^-$ (*purple*) incorporated. Corresponding experimental (A_1^- - A_1) FTIR DS are also shown (*dotted*). DS are calculated for $2MNQ^-$ oriented in the binding site with its methyl group meta/ortho to the H-bond (*blue/pink*). A frequency scaling factor of 0.964 is employed for all calculated spectra.

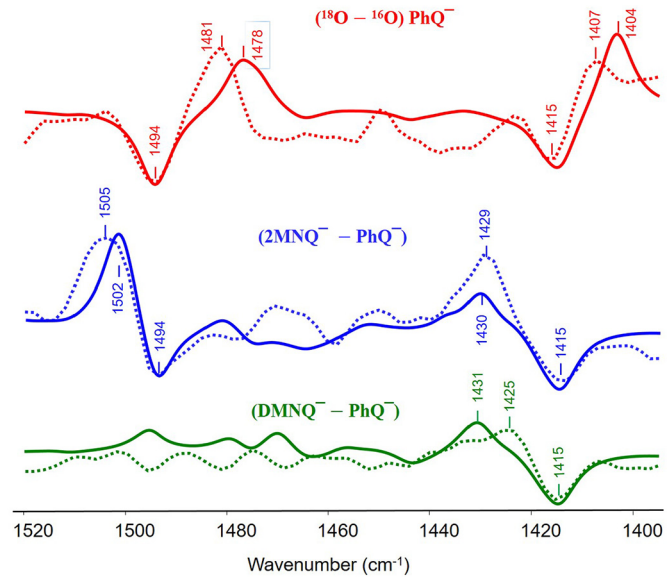

Fig. 3. ONIOM calculated (^{18}O – ^{16}O) (*red*), ($2MNQ^-$ – PhQ^-) (*blue*) and ($DMNQ^-$ – PhQ^-) (*green*) DDS. Corresponding experimental DDS are also shown (*dotted*). In the DDS bands of PhQ^- are negative while bands of the other semiquinones are positive.

Fig. S1. The standard error in the experimental DDS is also indicated in Fig. S1. The experimental DDS in the neutral region (1800–1550 cm^{-1}) do not show clear, unambiguous and easily assignable features, and it is for this reason that we focus on the semiquinone anion region in this manuscript.

Despite providing the framework to build our initial molecular model, the X-ray crystal structure does not directly provide structural information on the semiquinone state in the A_1 binding site. From the ONIOM calculated geometry optimized molecular structure, distances and angles associated with the semiquinones in the A_1 binding site are obtained and are listed in Table 1 (see also Fig. 1D). Table 1 indicates that the calculated $C_1 = O$ bond lengths are essentially the same for all three semiquinones, and the $C_4 = O$ bond is longer than the $C_1 = O$ bond for all three semiquinones. The PhQ^- $C_4 = O$ bond is longer than the $2MNQ^-$ or $DMNQ^-$ $C_4 = O$ bond.

The bands in the spectra in Figs. 2 and 3 are due to various normal modes. Table 2 lists the (highest intensity) calculated normal mode vibrational frequencies and the molecular groups that contribute most to the normal modes. Experimental band frequencies are also listed in Table 2.

4. Discussion

4.1. Unlabeled and ^{18}O-labeled PhQ^-

In the (^{18}O – ^{16}O) DDS in Fig. 3, the 1494 cm^{-1} band is calculated to

Table 1
ONIOM calculated bond lengths (in Å) and angles (in degrees) for PhQ^-, $2MNQ^-$, and $DMNQ^-$ in the A_1 binding site. The X-ray data for neutral PhQ is also shown. The 'X' refers to the various attachments at the C_3 position of the different naphthoquinones.

	$C_1{=}O$	$C_4{=}O$	$C_2 = C_3$	N - - O_4	$\angle(C_{methyl}\text{-}C_2\text{-}C_1)$	$\angle(X\text{-}C_3\text{-}C_4)$
X-ray	1.42	1.42	1.46	2.69	119.0	118.5
PhQ^-	1.26	1.29	1.391	2.64	116.8	116.5
$2MNQ^-$	1.26	1.28	1.382	2.68	118.2	115.8
$DMNQ^-$	1.26	1.28	1.391	2.67	117.3	117.5

Table 2
ONIOM calculated vibrational frequencies (in cm^{-1}) and intensities (in km/mol) for unlabeled and ^{18}O labeled PhQ^-, as well as for $2MNQ^-$ and $DMNQ^-$. Frequencies are scaled by 0.964. The molecular groups that most prominently contribute to the calculated vibrational modes are listed along with the experimentally determined band frequencies. ν/δ refer to stretching/bending modes. An animation/movie of the 1415 cm^{-1} mode of PhQ^- can be found in the Supplementary information.

Quinone	Mode	ν Calc. Freq. (Int.)	Exp.
PhQ^-	$\nu(C_1{=}O)$	1494 (341)	1494
	$\delta(CH_3)$ attached to C_2	1475 (75)	1476
	δ(CH) of the phytyl tail	1444 (68)	–
	$\nu(C_2{=}C_3)$	1435 (29)	–
	$\nu(C_4{=}O)$	1415 (239)	1415
^{18}O PhQ^-	$\nu(C_1{=}O)$	1478 (109)	1481
	$\delta(CH_3)$ attached to C_2	1474 (84)	–
	δ(CH) of the phytyl tail	1443 (33)	–
	$\nu(C_2{=}C_3)$	1434 (26)	–
	$\nu(C_4{=}O)$	1404 (366)	1407
$2MNQ^-$	$\nu(C_1{=}O)$	1502 (364)	1505
	$\delta(CH_3)$ attached to C_2	1481 (75)	–
	$\nu(C_4{=}O)$	1430 (162)	1429
$DMNQ^-$	$\nu(C_1{=}O)$	1494 (444)	1495
	$\delta(CH_3)$ attached C_2 & C_3	1480 (63)	–
	$\delta(CH_3)$ attached C_2 & C_3	1470 (152)	–
	$\nu(C_4{=}O)$	1431 (139)	1425

downshifts 16 cm^{-1} to 1478 cm^{-1}. The calculated bands at 1494 and 1478 cm^{-1} are due mainly to the non-H-bonded $C_1{=}O$ vibration of unlabeled and ^{18}O labeled PhQ^-, respectively (Table 2). The calculated 1494(−)/1478(+) cm^{-1} difference band in the DDS corresponds to the experimental 1494(−)/1481(+) cm^{-1} difference band. So the calculated ^{18}O-induced downshift of the $C_1{=}O$ mode of PhQ^- is 3 cm^{-1} larger than the observed downshift.

Similar results are obtained for PSI with unlabeled and ^{18}O-labeled 2MNQ incorporated, where the experimental band of unlabeled $2MNQ^-$ at 1504 cm^{-1} is observed to downshift 14 cm^{-1} to 1490 cm^{-1} upon ^{18}O labeling, in good agreement with the calculation which indicates a 13 cm^{-1} ^{18}O-induced downshift of the $C_1{=}O$ mode of $2MNQ^-$ (Fig. S2).

A negative band is observed at 1415 cm^{-1} in all three experimental DDS in Fig. 3, unambiguously indicating that it is due to a band of unlabeled PhQ^-. Experimentally, the 1415 cm^{-1} band of PhQ^- appears to downshift 8 cm^{-1} to 1407 cm^{-1} upon ^{18}O labeling (Fig. 3). A band of PhQ^- is also calculated at 1415 cm^{-1} and is predicted to downshifts 11 cm^{-1} to 1404 cm^{-1} upon ^{18}O labeling (Fig. 3). The calculations show that the negative/positive 1415/1404 cm^{-1} bands are due at least in part to the H-bonded $C_4{=}O$ group of PhQ^- (Table 2), in agreement with previous work [33].

Similar results are obtained for unlabeled and ^{18}O-labeled $2MNQ^-$ (Fig. S2), were a band of unlabeled $2MNQ^-$ at ~1429 cm^{-1} downshifts 8 cm^{-1} upon ^{18}O labeling. In corresponding calculations a band at 1430 cm^{-1} due in part to a $C_4{=}O$ mode downshifts 11 cm^{-1} upon ^{18}O labeling, in good agreement with experiment [62].

In the experimental PhQ^- DS in Fig. 2 a band is observed near 1476 cm^{-1}. A band is calculated at the same frequency. Calculations indicate that this band is mainly due to the methyl bending vibrational mode, and is thus not expected to be impacted upon ^{18}O labeling (Fig. 2 and Table 2). Previously it was suggested that a 1476 cm^{-1} band is due in part to a $C_4{=}O$ vibration. [43]. This suggestion was based on the results of calculations undertaken using a simple molecular model in gas-phase calculations. Based on the more sophisticated computational procedure used here, no $C_4{=}O$ vibration is calculated near a 1476 cm^{-1}, indicating inadequacies in the previous simpler calculations, and also indicating the importance of undertaking calculations that include the protein environment.

The calculated and experimental (^{18}O – ^{16}O) DDS indicate that it is mainly the 1494 and 1415 cm^{-1} bands that are impacted by ^{18}O labeling, and so there is little doubt that these two bands are due (at least in part) to the $C{=}O$ stretching vibrational modes of PhQ^-. Semiquinone $C{=}O$ modes are known to downshift ~15 cm^{-1} upon ^{18}O labeling [51] and this is found to be approximately correct for the 1495 cm^{-1} band. The 1415 cm^{-1} band downshifts only ~8 cm^{-1}, indicating a greater degree of mixing of the $C{=}O$ mode responsible for the 1415 cm^{-1} band. This conclusion is obvious from an animation of the 1415 cm^{-1} normal mode (see animation of 1415 cm^{-1} mode of PhQ^- in the Supplementary information).

Given that PhQ has a phytyl chain where DMNQ/2MNQ has a methyl group/hydrogen atom, respectively, it might be valuable to be able to identify bands that could be associated with the phytyl chain of PhQ (distinguishing one of the methyl groups of DMNQ would be difficult). In the calculated PhQ^- DS a band is found at 1444 cm^{-1}, that is mainly due to the C–H bending vibrations associated with the hydrocarbon tail of PhQ (Table 2). Upon ^{18}O labeling, a band is calculated at 1443 cm^{-1} with a similar mode composition but lower in intensity (Table 2). Given the relatively low intensity of this mode it is unlikely that such a band could be identified in the experimental spectrum. In the experimental DS a broad set of bands is observed near 1444 cm^{-1}, but no assignments have been made. Even in the calculated ($2MNQ^-$ – PhQ^-) and ($DMNQ^-$ – PhQ^-) DDS there is no clear indication of a negative band at 1444 cm^{-1}.

4.2. ($2MNQ^-$ – PhQ^-) DDS

The $C_1{=}O$ mode of $2MNQ^-$ gives rise to a positive band at 1505 cm^{-1} (Fig. 2 and Fig. S1), 11 cm^{-1} higher than the corresponding band of PhQ^- (Fig. 2). These features give rise to the 1505(+)/1494(−) cm^{-1} difference band in the experimental ($2MNQ^-$ – PhQ^-) DDS. A difference band is calculated at 1502(+)/1494(−) cm^{-1} (Fig. 3), suggesting an upshift of ~8 cm^{-1} for the $C_1{=}O$ mode of $2MNQ^-$ relative to that of PhQ^-. Again, the calculations agree well with experiment, but are not necessarily an improvement over previous three-layer ONIOM calculations, at least on this point [40].

The experimental ($2MNQ^-$ – PhQ^-) DDS gives rise to a difference band at 1415(−)/1429(+) cm^{-1}, very similar to that calculated (Fig. 3). The calculations show that the 1415(−)/1430(+) cm^{-1} band is due to $C_4{=}O$ mode of PhQ^-/$2MNQ^-$, respectively. Fig. S2 in the Supplementary information shows calculated and experimental FTIR DS for PSI with unlabeled and ^{18}O labeled $2MNQ^-$ incorporated, which also support the idea that the 1415(−)/1430(+) cm^{-1} band of PhQ^-/$2MNQ^-$ is due to a $C_4{=}O$ mode, respectively.

Of particular note here is that in previous three-layer ONIOM calculations this aspect of the experimental data could not be modeled [40]. In previous three-layer ONIOM calculations the predominantly $C_4{=}O$ vibrational mode of PhQ^- and $2MNQ^-$ were both calculated to be at 1426 cm^{-1}, with the $2MNQ^-$ mode being 2.3 times more intense than the corresponding PhQ^- mode [40], which does not agree with experiment. So, the current computational method is superior, or is an improvement, over the three-layer ONIOM method considered previously [40], at least on this point.

ONIOM calculations were also undertaken for $2MNQ^-$ oriented with its methyl group ortho to the H-bond. The calculated DS for $2MNQ^-$ with this orientation is also shown in Fig. 2 (*pink*). The calculated band pattern in the DS for of $2MNQ^-$ with its methyl group ortho to the H-bond is very different than that obtained for $2MNQ^-$ with its methyl group meta to the H-bond (Fig. 2), and does not agree with the experimental DS. Therefore, based on a comparison of the calculated and experimental DS, we can rule out the possibility that $2MNQ^-$ adopts an orientation with the methyl group ortho to the H-bond. This agrees with conclusions drawn from EPR experiments on PSI with 2MNQ incorporated [52,53].

4.3. ($DMNQ^-$ – PhQ^-) DDS

An intense negative band is observed at 1494 cm^{-1} in the experimental (^{18}O – ^{16}O) and ($2MNQ^-$–PhQ^-) DDS. As suggested above, this band is due to the C_1=O mode of PhQ^-. A band at 1494 cm^{-1} is not observed in the experimental ($DMNQ^-$ – PhQ^-) DDS. Notably, no 1494 cm^{-1} band is observed in the calculated DDS either.

The lack of a band at 1494 cm^{-1} in the ($DMNQ^-$ – PhQ^-) DDS indicates that $DMNQ^-$ also gives rise to a band at 1494 cm^{-1}. Such a band is clear in the experimental DS in Fig. 2, and calculations on $DMNQ^-$ in the A_1 binding site also predict a band for $DMNQ^-$ at 1494 cm^{-1}, and that this band is due to a C_1=O vibrational mode (Table 2).

The difference feature at 1415(−)/1425(+) cm^{-1} in the experimental ($DMNQ^-$ – PhQ^-) DDS in Fig. 3 indicates that the C_4=O mode for $DMNQ^-$ is 10 cm^{-1} higher than that for PhQ^-.

This might be unexpected given the similarity of the FTIR absorption spectra of neutral PhQ and DMNQ in THF [54], and the similarity in frequency of the C_1=O mode of both $DMNQ^-$ and PhQ^- discussed above. However, the calculations also indicate that the C_4=O mode of $DMNQ^-$ is upshifted (14 cm^{-1}) compared to PhQ^-.

The fact that the calculations exhibit the same trend as the experiment, supports the applicability of the computational procedure used here. In fact, one reason we find the current computational approach appealing is that it captures experimental spectral features observed for PSI with both 2MNQ and DMNQ incorporated, as well as the features in the isotope edited DDS. Something that previous ONIOM type calculations were not able to do [33,40].

Finally, given that $DMNQ^-$ and PhQ^- exhibit a C_1=O mode vibration at the same frequency, but the C_4=O modes are at different frequencies, indicates coupling between the C_4=O group (but not the C_1=O group) of PhQ^- with groups of the phytyl chain. This seems reasonable given that the C_4=O group is ortho to the phytyl chain (Fig. 1B, also see Movie of the 1415 cm^{-1} mode of PhQ^- in the Supplementary information).

In summary, the location of the positive band in the 1415–1430 cm^{-1} region in (A_1^- - A_1) FTIR DS (Fig. 2) can be used to distinguish if PhQ, 2MNQ or DMNQ is in the A_1 binding site.

4.4. H-bond strength

The calculated and experimental spectra presented here indicate an ~80 cm^{-1} separation in frequency between the C_1=O and C_4=O vibrational modes, for all three semiquinones in the A_1 binding site. This splitting is due in part to strong H-bonding between the NH backbone of LeuA722 and the C_4=O oxygen atom (Fig. 1B). Such a large shift could suggest an exceedingly strong H-bond. However, the mode that we associate with the C_4=O group is a complex vibration (see Movie in the Supplementary information), exhibiting considerable mixing with other molecular groups. As discussed previously [40], it is probably unwise to assign and discuss molecular modes as if they were due to isolated (unmixed) C_4=O and C_1=O molecular groups.

The excellent agreement between the calculated and experimental DS and DDS (Figs. 2, 3) demonstrates the appropriateness of the molecular structural model developed and the computational procedures used. It is important to note that in the calculations reported here none of the amino acid residues neighboring the non-H-bonded C_1=O group were modeled at the QM level. Thus, these residues, as well as the nearby H-bond network involving water molecules numbered 5, 6 and 7 in Fig. 1C, are less critical regarding simulating the FTIR DS and DDS.

None of the seven water molecules outlined in Fig. 1C are within ~4 Å of the NH backbone of LeuA722, although three (1, 2, and 3) are within 3.6 Å of the backbone atoms of AlaA721 and SerA723 (Fig. 4). Such distances suggest H-bonding is likely between these water molecules and the protein backbone atoms [55,56] (see Section 4 in the Supplementary information).

In Figs. S3 and S4 we compare ($2MNQ^-$ – PhQ^-) DDS calculated using molecular models with different numbers of water molecules considered in the QM layer. If none of the seven water molecules are treated at the QM level (Model 0), the calculated and experimental DDS do not agree (Fig. S3), particularly concerning the 1415(−)/1429(+) cm^{-1} difference feature that is associated with the C_4=O vibrational mode. The DDS that was calculated previously using a three-layer ONIOM method also showed poor agreement with experimental DDS concerning this spectral feature [40]. In these previous three-layer ONIOM calculations, no water molecules were included in the molecular model [40].

The calculated ($2MNQ^-$ – PhQ^-) DDS with different numbers of water molecules included in the QM layer show that the best agreement between calculated and experimental DDS is found when the three water molecules, numbered (1), (2) and (3) (see numbering in Figs. 1B, C and 4) are included at the QM level (Figs. S3 and S4). Including water molecule (4), or more, does not improve the agreement between the calculated and experimental DDS (Fig. S3). The molecular model that includes water molecules (1), (2) and (3) at the QM level also results in calculated (^{18}O – ^{16}O) and ($DMNQ^-$ – PhQ^-) DDS that are in excellent agreement with experiment (Fig. 3).

The calculated ($2MNQ^-$ – PhQ^-) DDS in Figs. S3 and S4 were obtained using molecular models with different numbers of water molecules in the QM layer, and indicates that both the C_1=O and C_4=O vibrational modes are sensitive to the surrounding water molecules, in spite of the fact that none of these water molecules directly H-bond to the C=O groups.

In the calculations here for PhQ^- the distance between the backbone nitrogen of LeuA722 and the oxygen atom of PhQ^- is 2.64 Å. This distance is considerably less than the 2.69 Å found for neutral PhQ in the X-ray structure (Table 1). This distance is in fact the smallest calculated for all of the different molecular models with different numbers of water molecules at the QM level (Fig. S5). For a donor-acceptor distance of 2.64 Å this H-bond could be classified as moderately strong and mostly electrostatic in nature [56] (see Supplementary information Section 5). In moderately strong, mostly electrostatic H-bonds, the hydrogen atom does not lie on a straight line connecting the hydrogen donor to acceptor [56]. PSI X-ray crystal structures indicate the H-bond displays an out of plane angle of ~33° [12,57,58], while our calculations for PhQ^- indicate 37° (Fig. 1D).

The distance between the C_4=O oxygen atom of PhQ and the hydrogen atom of the NH backbone of LeuA722 (O…H distance) in the calculations presented here is ~1.59 Å. This calculated distance agrees well with the 1.6 ± 0.1 Å distance estimated from HYSCORE experiments where PhQ^- was photoaccumulated under reducing conditions at low temperature [57]. Although the agreement between our calculations and the HYSCORE experiments appears to be excellent, we point out that we also calculate similar O…H distances for molecular models with different numbers of water molecules included in the QM level (Fig. S6). In previously reported DFT calculations the O…H distance and out of the plane angle were calculated to be 1.56 Å and 35°, respectively [58].

ONIOM type QM:MM methods have been used previously in order to calculate the EPR parameters for PhQ^- in the A_1 binding site [59]. Many molecular models, with the QM layer ranging in size by adding specific amino acids, were considered. The calculated EPR parameters obtained from many of these molecular models were in good agreement with experiment [63]. The question that arises then is do these molecular models also adequately account for the measured FTIR DS. We have used the largest model considered in the previous EPR ONIOM calculations (model *f* in reference [59]) in order to calculate FTIR DS for PSI with different quinones incorporated. The molecular model used, and calculated ($2MNQ^-$ – PhQ^-) and ($DMNQ^-$ – PhQ^-) DDS, are shown in Fig. S7. Calculated FTIR DS obtained using the same molecular model *f* as in reference [59] are also outlined in reference [60]. Comparison of the calculated and experimental DDS in Fig. S7

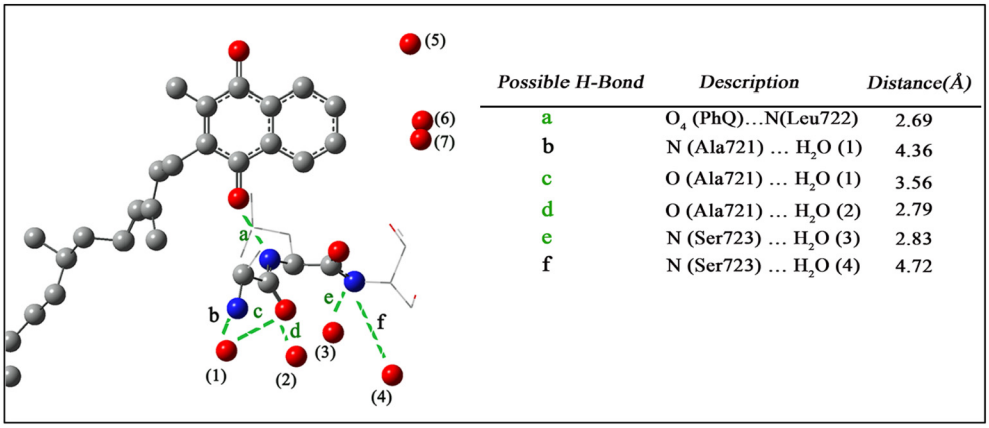

Possible H-Bond	Description	Distance(Å)
a	O_4 (PhQ)…N(Leu722)	2.69
b	N (Ala721) … H_2O (1)	4.36
c	O (Ala721) … H_2O (1)	3.56
d	O (Ala721) … H_2O (2)	2.79
e	N (Ser723) … H_2O (3)	2.83
f	N (Ser723) … H_2O (4)	4.72

Fig. 4. View of the water molecules that are near PhQ in PSI. Possible H-bond distances are listed. Structure and distances are taken from the PSI crystal structure at 2.5 Å resolution (PDB 1JB0) [12]. Water molecules (5), (6), and (7) were included in the MM layer in ONIOM calculations. The distances labeled 'b' and 'f' are longer than what might be considered appropriate for an H-bond. Water molecule numbering as in Fig. 1.

demonstrates that the molecular models used previously to calculate the EPR parameters cannot be used to adequately simulate all of the FTIR DDS. On the other hand, however, the ONIOM model outlined in this manuscript (used to calculate FTIR DDS) yields EPR parameters that are similar to that calculated previously (Table S2).

The work presented here indicates that three specific water molecules must be included in the molecular model to correctly simulate all of the experimental spectra. These water molecules are found in both the A_{1A} and A_{1B} binding sites, and are conserved in all PSI crystal structures. It has been proposed that these water molecules help strengthen and stabilize the backbone H-bond [61]. The spectra presented here indicate a strong backbone H-bond is present for PSI with all three quinones incorporated. The incorporated quinones have different substitutions, and the presence of a similar H-bond in all three cases indicates a highly stable H-bond. One way to stabilize (and strengthen) the backbone H-bond is to bolster the immediate backbone via a network of H-bonding water molecules. Water molecules 1–3 behind the LeuA722 residue are in position to do this. If the H-bonding network of water molecules do contribute to the strength and stability of the H-bond to PhQ, then this will also impact the functioning of PhQ in the A_1 binding site, as a stronger H-bonding will make the PhQ redox potential more positive. In this way, one can see how FTIR difference band frequencies and molecular structure can be related to the functional characteristics of the quinones bound in the A_1 binding site.

5. Conclusions

We have used a two-layer ONIOM method to calculate several DS and DDS associated with different semiquinones in the A_1 binding site. Calculations were undertaken for a range of molecular models with different numbers of water molecules included or excluded from the QM layer. The best molecular model was identified based on how well the calculated and experimental spectra agreed. We found a molecular model that included three specific water molecules at the QM level gave the best agreement between calculated and experimental spectra.

From comparing calculated and experimental DS and DDS obtained using PSI with PhQ, 2MNQ and DMNQ incorporated, and also specifically ^{18}O isotope labeled PhQ and 2MNQ incorporated, we found:

1. For PhQ^- and $2MNQ^-$, only two semiquinone bands were found to shift upon ^{18}O labeling. These bands are due to the $C_1 \doteqdot O$ and $C_4 \doteqdot O$ groups. For PhQ^-, these bands are at 1494 and 1415 cm^{-1}, respectively. For $2MNQ^-$ these bands are at 1505 and 1429 cm^{-1}, respectively. The calculated ^{18}O induced frequency shifts agree well with experiment. The ^{18}O induced frequency downshift of the $C_4 \doteqdot O$ group is considerably smaller than that of the $C_1 \doteqdot O$ group, indicating that the mode we associate with the $C_4 \doteqdot O$ group is considerably mixed with other molecular groups.
2. For $DMNQ^-$ bands associated with the $C_1 \doteqdot O$ and $C_4 \doteqdot O$ groups are found at 1494 and 1425 cm^{-1}, respectively. So the $C_1 \doteqdot O$ mode of PhQ^- and $DMNQ^-$ are at the same frequency, while the $C_4 \doteqdot O$ mode of $DMNQ^-$ is at a higher frequency, which could be expected as the $C_4 \doteqdot O$ mode of PhQ^- could contain contributions from molecular groups of the phytyl chain.
3. Four different experimental DDS were presented in this manuscript. The calculated DDS agree well with all four experimental DDS. No other calculations that have ever been undertaken could model all four of these DDS simultaneously. In this respect the computational procedures outlined here are a significant advance.
4. All of the calculated and experimental spectra support the idea of a significant frequency separation between the carbonyl groups of the semiquinones, indicating a strong asymmetric H-bonding for the semiquinones.
5. Spectra were calculated for the two possible orientations that 2MNQ could adopt in the A_1 binding site. From a comparison of these calculated spectra with experimental spectra we were able to establish which orientation 2MNQ adopts in the A_1 binding site.
6. The semiquinone band in the 1415–1430 cm^{-1} region is a marker for the type of quinone in the binding site.
7. Water molecules in the neighborhood of the H-bonded carbonyl group (the $C_4{=}O$ group) directly influence the calculated infrared spectra. Our calculations indicate that three specific water molecules are of particular importance, probably providing a structural factor that could increase the H-bond strength.

Supplementary data to this article can be found online at https://doi.org/10.1016/j.bbabio.2019.07.003.

Transparency document

The Transparency document associated with this article can be found, in online version.

Acknowledgements

This material is based upon work supported by the U.S. Department of Energy, Office of Science, Office of Basic Energy Sciences, under Award Number DE-SC-0017937 to GH. We acknowledge the use of Georgia State's research computing resources that are supported by Georgia State's Research Solutions. We thank Dr. Samer Gozem for useful discussions. The statements made herein are solely the responsibility of the authors.

References

[1] D. Walker, Energy, plants and man, 2nd ed ed., Oxygraphics, Brighton, East Sussex: Mill Valley, CA (1993).

[2] M. Guergova-Kuras, B. Boudreaux, A. Joliot, P. Joliot, K. Redding, Evidence for two active branches for electron transfer in photosystem I, Proc. Natl. Acad. Sci. U. S. A. 98 (2001) 4437–4442.

[3] K. Brettel, W. Leibl, Electron transfer in photosystem I, Bba-Bioenergetics 1507 (2001) 100–114.

[4] K. Brettel, Electron transfer and arrangement of the redox cofactors in photosystem I, Biochim. Biophys. Acta 1318 (1997) 322–373.

[5] H. Makita, N. Zhao, G. Hastings, Time-resolved visible and infrared difference spectroscopy for the study of photosystem I with different quinones incorporated into the A_1 binding site, Biochimica et Biophysica Acta (BBA) - Bioenergetics 1847 (2015) 343–354.

[6] K. Kawashima, H. Ishikita, Structural factors that alter the redox potential of quinones in cyanobacterial and plant photosystem I, Biochemistry 56 (2017) 3019–3028.

[7] K. Redding, A. van der Est, The directionality of electron transport in photosystem I, in: J. Golbeck (Ed.), Photosystem I: The Light Driven Plastocyanin:Ferredoxin Oxidoreductase, Springer, Dordrecht, 2006, pp. 413–437.

[8] J. Golbeck, D. Bryant, Photosystem I, Academic Press, New York, Current Topics in Bioenergetics, 1991, pp. 83–175.

[9] N. Srinivasan, J.H. Golbeck, Protein-cofactor interactions in bioenergetic complexes: the role of the A(1A) and A(1B) phylloquinones in photosystem I, Biochimica et Biophysica Acta (BBA) - Bioenergetics 1787 (2009) 1057–1088.

[10] C.S. Coates, J. Ziegler, K. Manz, J. Good, B. Kang, S. Milikisiyants, R. Chatterjee, S.J. Hao, J.H. Golbeck, K.V. Lakshmi, The structure and function of quinones in biological solar energy transduction: a cyclic voltammetry, EPR, and hyperfine sublevel correlation (HYSCORE) spectroscopy study of model naphthoquinones, J. Phys. Chem. B 117 (2013) 7210–7220.

[11] P. Fromme, P. Jordan, N. Krauss, Structure of photosystem I, Biochim. Biophys. Acta 1507 (2001) 5–31.

[12] P. Jordan, P. Fromme, H.T. Witt, O. Klukas, W. Saenger, N. Krauss, Three-dimensional structure of cyanobacterial photosystem I at 2.5 angstrom resolution, Nature 411 (2001) 909–917.

[13] Y. Mazor, A. Borovikova, N. Nelson, The structure of plant photosystem I supercomplex at 2.8 A resolution, Elife, 4 (2015) e07433.

[14] Y. Mazor, D. Nataf, H. Toporik, N. Nelson, Crystal structures of virus-like photosystem I complexes from the mesophilic cyanobacterium Synechocystis PCC 6803, Elife 3 (2013) e01496.

[15] W. Mantele, Reaction-induced infrared difference spectroscopy for the study of protein function and reaction mechanisms, Trends Biochem. Sci. 18 (1993) 197–202.

[16] W. Mäntele, Infrared vibrational spectroscopy of photosynthetic reaction centers, in: J. Deisenhofer, J. Norris (Eds.), The Photosynthetic Reaction Center, Academic Press, San Diego, 1993, pp. 239–283.

[17] W. Mäntele, Infrared vibrational spectroscopy of reaction centers, in: R.E. Blankenship, M.T. Madigan, C.E. Bauer (Eds.) Anoxygenic Photosynthetic Bacteria, Kluwer Academic Publishers, Dordrecht; Boston (1995) pp. 627–647.

[18] E. Nabedryk, Light-induced Fourier transform infrared difference spectroscopy of the primary electron donor in photosynthetic reaction centers, in: H.H. Mantsch, D. Chapman (Eds.), Infrared Spectroscopy of Biomolecules, Wiley-Liss, New York, 1996, pp. 39–81.

[19] J. Breton, E. Nabedryk, Protein-quinone interactions in the bacterial photosynthetic reaction center: light-induced FTIR difference spectroscopy of the quinone vibrations, Biochim. Biophys. Acta 1275 (1996) 84–90.

[20] T. Domratcheva, E. Hartmann, I. Schlichting, T. Kottke, Evidence for Tautomerisation of Glutamine in BLUF Blue Light Receptors by Vibrational Spectroscopy and Computational Chemistry, Scientific Reports, 6, (2016).

[21] C. Thoing, A. Pfeifer, S. Kakorin, T. Kottke, Protonated triplet-excited flavin resolved by step-scan FTIR spectroscopy: implications for photosensory LOV domains, Phys. Chem. Chem. Phys. 15 (2013) 5916–5926.

[22] K. Noguchi, Molecular analysis by vibrational spectroscopy, in: T. Wydrzynski, K. Satoh, J. Freeman (Eds.), Photosystem II - The Light-driven Water:Plastoquinone Oxidoreductase, Springer, The Netherlands, 2005, pp. 367–387.

[23] P. Hellwig, Vibrational spectroscopies and bioenergetic systems, Biochim. et Biophys. Acta (Bioenergetics) (Special Issue) 1847 (2015) 1–142.

[24] K.J. Rothschild, FTIR difference spectroscopy of bacteriorhodopsin: toward a molecular model, J. Bioenerg. Biomembr. 24 (1992) 147–167.

[25] M.S. Braiman, K.J. Rothschild, Fourier transform infrared techniques for probing membrane protein structure, Annu. Rev. Biophys. Biophys. Chem. 17 (1988) 541–570.

[26] W. Uhmann, A. Becker, C. Taran, F. Siebert, Time-resolved FT-IR absorption spectroscopy using a step-scan interferometer, Appl. Spectrosc. 45 (1991) 390–397.

[27] G. Hastings, Time-resolved step-scan Fourier transform infrared and visible absorption difference spectroscopy for the study of photosystem I, Appl. Spectrosc. 55 (2001) 894–900.

[28] G. Hastings, FTIR studies of the intermediate electron acceptor A_1, in: J. Golbeck (Ed.), Photosystem I: The Light Driven Plastocyanin:Ferredoxin Oxidoreductase, Springer, Dordrecht, 2006, pp. 301–318.

[29] K. Gerwert, Time-resolved FT-IR difference spectroscopy: a tool to monitor molecular reaction mechanisms of proteins, in: H. Gremlich, B. Yan (Eds.), Infrared and Raman Spectroscopy of Biological Materials, Marcel Dekker, New York, 2001, pp. 193–230.

[30] S.E. Plunkett, J.L. Chao, T.J. Tague, R.A. Palmer, Time-resolved step-scan Ft-Ir spectroscopy of the photodynamics of carbonmonoxymyoglobin, Appl. Spectrosc. 49 (1995) 702–708.

[31] C. Kotting, K. Gerwert, Proteins in action monitored by time-resolved FTIR spectroscopy, Chemphyschem 6 (2005) 881–888.

[32] T. Kottke, V.A. Lorenz-Fonfria, J. Heberle, The grateful infrared: sequential protein structural changes resolved by infrared difference spectroscopy, J. Phys. Chem. B 121 (2017) 335–350.

[33] G. Hastings, Vibrational spectroscopy of photosystem I, Biochimica et Biophysica Acta (BBA) - Bioenergetics 1847 (2015) 55–68.

[34] V.A. Lorenz-Fonfria, J. Heberle, Proton Transfer and Protein Conformation Dynamics in Photosensitive Proteins by Time-resolved Step-scan Fourier-transform Infrared Spectroscopy, Jove-J Vis Exp (2014).

[35] C. Zscherp, J. Heberle, Infrared difference spectra of the intermediates L, M, N, and O of the bacteriorhodopsin photoreaction obtained by time-resolved attenuated total reflection spectroscopy, Journal of Physical Chemistry B 101 (1997) 10542–10547.

[36] K. Bandaranayake, R. Wang, G. Hastings, Modification of the phylloquinone in the A_1 binding site in photosystem I studied using time-resolved FTIR difference spectroscopy and density functional theory, Biochemistry 45 (2006) 4121–4127.

[37] H.P. Lamichhane, G. Hastings, Calculated vibrational properties of pigments in protein binding sites, Proc. Natl. Acad. Sci. U. S. A. 108 (2011) 10526–10531.

[38] L.M. Thompson, A. Lasoroski, P.M. Champion, J.T. Sage, M.J. Frisch, J.J. van Thor, M.J. Bearpark, Analytical harmonic vibrational frequencies for the green fluorescent protein computed with ONIOM: chromophore mode character and its response to environment, J. Chem. Theory Comput. 10 (2014) 751–766.

[39] L.W. Chung, W.M.C. Sameera, R. Ramozzi, A.J. Page, M. Hatanaka, G.P. Petrova, T.V. Harris, X. Li, Z.F. Ke, F.Y. Liu, H.B. Li, L.N. Ding, K. Morokuma, The ONIOM method and its applications, Chem. Rev. 115 (2015) 5678–5796.

[40] H. Makita, L. Rohani, N. Zhao, G. Hastings, Quinones in the A_1 binding site in photosystem I studied using time-resolved FTIR difference spectroscopy, Biochimica et Biophysica Acta (BBA) - Bioenergetics 1858 (2017) 804–813.

[41] G. Hastings, K.M.P. Bandaranayake, E. Carrion, Time-resolved FTIR difference spectroscopy in combination with specific isotope labeling for the study of A(1), the secondary electron acceptor in photosystem 1, Biophys. J. 94 (2008) 4383–4392.

[42] R. Schmid, F. Goebel, A. Warnecke, A. Labahn, Synthesis and redox potentials of methylated vitamin K derivatives, J Chem Soc Perk T 2 (1999) 1199–1202.

[43] H. Makita, G. Hastings, Time-resolved step-scan FTIR difference spectroscopy for the study of photosystem I with different benzoquinones incorporated into the A1 binding site, Biochimica et Biophysica Acta (BBA) - Bioenergetics 1859 (2018) 1199–1206.

[44] J.J. Snellenburg, S.P. Laptenok, R. Seger, K.M. Mullen, I.H.M. van Stokkum, Glotaran: a Java-based graphical user interface for the R package TIMP, J. Stat. Softw. 49 (2012) 1–22.

[45] R. Dennington, T.A. Keith, J.M. Millam, GaussView, Version 6 (2016).

[46] M.J. Frisch, G.W. Trucks, H.B. Schlegel, G.E. Scuseria, M.A. Robb, J.R. Cheeseman, G. Scalmani, V. Barone, G.A. Petersson, H. Nakatsuji, X. Li, M. Caricato, A.V. Marenich, J. Bloino, B.G. Janesko, R. Gomperts, B. Mennucci, H.P. Hratchian, J.V. Ortiz, A.F. Izmaylov, J.L. Sonnenberg, Williams, F. Ding, F. Lipparini, F. Egidi, J. Goings, B. Peng, A. Petrone, T. Henderson, D. Ranasinghe, V.G. Zakrzewski, J. Gao, N. Rega, G. Zheng, W. Liang, M. Hada, M. Ehara, K. Toyota, R. Fukuda, J. Hasegawa, M. Ishida, T. Nakajima, Y. Honda, O. Kitao, H. Nakai, T. Vreven, K. Throssell, J.A. Montgomery Jr., J.E. Peralta, F. Ogliaro, M.J. Bearpark, J.J. Heyd, E. N. Brothers, K.N. Kudin, V.N. Staroverov, T.A. Keith, R. Kobayashi, J. Normand, K. Raghavachari, A.P. Rendell, J.C. Burant, S.S. Iyengar, J. Tomasi, M. Cossi, J.M. Millam, M. Klene, C. Adamo, R. Cammi, J.W. Ochterski, R.L. Martin, K. Morokuma, O. Farkas, J.B. Foresman, D.J. Fox, Gaussian 16 Rev. B.01, Wallingford, CT (2016).

[47] K. Bandaranayake, V. Sivakumar, R. Wang, G. Hastings, Modeling the A_1 binding site in photosystem I. Density functional theory for the calculation of "anion – neutral" FTIR difference spectra of phylloquinone, Vib. Spectrosc. 42 (2006) 78–87.

[48] H.P. Lamichhane, G. Hastings, Calculated vibrational properties of ubisemiquinones, Computational Biology Journal 2013 (2013) 11.

[49] A.K. Rappe, C.J. Casewit, K.S. Colwell, W.A. Goddard, W.M. Skiff, Uff, a full periodic-table force-field for molecular mechanics and molecular-dynamics simulations, J. Am. Chem. Soc. 114 (1992) 10024–10035.

[50] V. Sivakumar, R. Wang, G. Hastings, A1 reduction in intact cyanobacterial photosystem I particles studied by time-resolved step-scan Fourier transform infrared difference spectroscopy and isotope labeling, Biochemistry 44 (2005) 1880–1893.

[51] M. Bauscher, W. Mantele, Electrochemical and infrared-spectroscopic characterization of redox reactions of p-quinones, J. Phys. Chem. 96 (1992) 11101–11108.

[52] A. van der Est, Y. Pushkar, I. Karyagina, B. Fonovic, T. Dudding, J. Niklas, W. Lubitz, J.H. Golbeck, Incorporation of 2,3-disubstituted-1,4-naphthoquinones into the A(1) binding site of photosystem I studied by EPR and ENDOR spectroscopy, Appl. Magn. Reson. 37 (2010) 65–83.

[53] Y. Pushkar, S. Zech, D. Stehlik, S. Brown, A. van der Est, H. Zimmermann, Orientation and protein-cofactor interactions of monosubstituted n-alkyl naphthoquinones in the A_1 binding site of photosystem I, J. Phys. Chem. B 106 (2002) 12052–12058.

[54] J. Breton, J.R. Burie, C. Boullais, G. Berger, E. Nabedryk, Binding sites of quinones in photosynthetic bacterial reaction centers investigated by light-induced FTIR difference spectroscopy: binding of chainless symmetrical quinones to the Q_A site of Rhodobacter sphaeroides,Biochemistry (1994) 12405–12415.

[55] E. Martz, Protein explorer: easy yet powerful macromolecular visualization, Trends Biochem. Sci. 27 (2002) 107–109.

[56] G. Jeffrey, An Introduction to Hydrogen Bonding, Oxford University Press, New York, Oxford, 1997.

[57] N. Srinivasan, R. Chatterjee, S. Milikisiyants, J.H. Golbeck, K.V. Lakshmi, Effect of hydrogen bond strength on the redox properties of phylloquinones: a two-dimensional hyperfine sublevel correlation spectroscopy study of photosystem I, Biochemistry 50 (2011) 3495–3501.

[58] C. Teutloff, W. Hofbauer, S.G. Zech, M. Stein, R. Bittl, W. Lubitz, High-frequency

EPR studies on cofactor radicals in photosystem I, Appl. Magn. Reson. 21 (2001) 363–379.
[59] T.J. Lin, P.J. O'Malley, Binding site influence on the electronic structure and electron paramagnetic resonance properties of the phyllosemiquinone free radical of photosystem I, J. Phys. Chem. B 115 (2011) 9311–9319.
[60] N. Zhao, Vibrational Properties of Quinones in Photosynthetic Reaction Centers, Georgia State University, Atlanta, GA, Physics and Astronomy, 2014.
[61] Y.N. Pushkar, J.H. Golbeck, D. Stehlik, H. Zimmermann, Asymmetric hydrogen-bonding of the quinone cofactor in photosystem I probed by C-13-labeled naphthoquinones, J. Phys. Chem. B 108 (2004) 9439–9448.
[62] G. Hastings, K.M.P. Bandaranayake, Quinone anion bands in A_1^-/A_1 FTIR difference spectra investigated using photosystem I particles with specifically labeled Naphthoquinones incorporated into the A_1 binding site, in: J. Allen, E. Gantt, J. Golbeck, B. Osmond (Eds.) Photosynthesis. Energy From the Sun. 14th International Congress on Photosynthesis Research 2007., Springer (2008) pp. Chapter 12 69–72.
[63] J. Niklas, B. Epel, M.L. Antonkine, S. Sinnecker, M.E. Pandelia, W. Lubitz, Electronic structure of the quinone radical anion A(1)(center dot-) of photosystem I investigated by advanced pulse EPR and ENDOR techniques, J. Phys. Chem. B 113 (2009) 10367–10379.